JOINT MAGNITUDE AND PHASE PROPERTIES OF NUMERICALLY SIMULATED HIGH-RESOLUTION VV- AND HH-POLARIZED X-BAND SEA BACKSCATTER OVER WIDE RANGE OF INCIDENCE ANGLES

Jakov V. Toporkov and Mark A. Sletten

Remote Sensing Division, Naval Research Laboratory, Washington DC, 20375-5320, USA

ABSTRACT

Joint properties of high-resolution coherent sea surface backscatter at different polarizations are studied using two-dimensional (2-D) direct numerical simulations based on a first-principles boundary integral equation technique. The quantities considered include the joint probability density function for HH and VV intensities and the distribution for the phase difference between the two polarization channels. Various distribution moments and polarimetric parameters such as entropy and "alpha angle" are also examined, including their sensitivity to wind speed and noise. A broad span of incidence angles (ranging from 20 to 85 degrees) is considered, which helps elucidate the trends as backscattering geometry evolves towards low grazing regime.

Index Terms— numerical simulations, sea surface electromagnetic scattering, clutter statistics, radar polarimetry.

1. INTRODUCTION

Sea surface backscatter occurs in many radar applications. Understanding and adequate description of its characteristics are often vital to performance and have been an active area of research. As radar systems increasingly adopt dual-polarization and full-polarization capabilities, more comprehensive properties of ocean backscatter become of interest. Such characteristics include joint probability distributions of magnitudes and phases in different polarization channels as well as aggregate statistics such as inter-channel correlations. The latter can be used to derive quantities such as entropy and "$\bar{\alpha}$-angle" that have been popular in radar polarimetry.

We investigate these sea backscatter properties using direct numerical scattering simulations [1]. The technique is based on solving the first-principles boundary integral equation for the induced electric current on the surface. The sea-like surfaces themselves are modeled as realizations of Gaussian random process characterized by a wind-driven wave spectrum, with accounting for lowest-order wave-wave interactions. The technique is computationally intensive and is limited to the 2-D space. Therefore, it can produce only co-polarized components of scattering matrix, corresponding to signals both transmitted and received at vertical (VV) and horizontal (HH) polarizations. Still, the ability of the numerical experiment to produce noise-free, well-calibrated dual-channel complex sea backscatter under highly-controlled conditions offers versatile and rather unique opportunities for high-fidelity analysis.

The low grazing angle (LGA) regime has been of a particular interest in surface scattering studies, for both practical and conceptual reasons. Such viewing geometry occurs in many coastal and shipborne radar applications, yet the LGA clutter exhibits a number of properties that are not reproduced or explained by the prevalent scattering theories that enjoy apparent success at moderate incidences. In the present simulations, we consider incidence angles varying from 20^o to 85^o from nadir. Such a broad range provides a more comprehensive look at the sea clutter behavior and helps elucidate tendencies as the low grazing regime is approached.

2. NUMERICAL SIMULATION DETAILS

The 2-D space simulations follow the general scheme described in [1]. Electromagnetic field, scattered by a given surface profile is calculated exactly, using a frequency-domain boundary integral equation technique. The equation can be efficiently solved by iterations using the Method of Ordered Multiple Interactions, also known as "Forward-backward"; further acceleration can be achieved by applying spectral expansions to the kernels (propagators) [2]. The incident field at the surface acts as a forcing term and can be computed in general based on the source location. In this study, we follow [1] in assuming the incident field to be a tapered plane wave, with the incidence angle being the major characteristic. Once the total induced current on the surface is determined, the scattered field anywhere in the upper half-space can be calculated as its radiation effect, i.e. by applying the appropriate propagator. We will focus on the far field in the backscattering direction. The frequency-domain formulation assumes that all fields and currents are time-harmonic. To achieve range resolution, the simulations are performed for a number of frequencies (1024 in all) covering the band of more than 1 GHz around f_0=9.3 GHz (λ_0=3.22 cm). Application of a spectral window combined with the inverse Fourier transform results in the synthesized surface response to a short pulse with a prescribed envelope

[1]. With the choice of the Harris-Nutall spectral weighing yielding very low sidelobe levels, the resulting pulse width is 0.4 m in magnitude (0.3 m in power).

A surface profile from which backscatter is calculated is generated as a realization of the Gaussian random process with the power spectral density modeled after the fully developed Elfouhaily wave spectrum [3]. The latter is parametrized by the wind speed at the 10-m height above the surface. We consider wind speeds of 5 and 7 m/s (rms surface heights 0.16 m and 0.32 m, respectively). To account for wave-wave interactions, a non-linear transformation by Creamer et al [4] is applied. While it does not lead to wave breaking, interactions of ripples with orbital currents of larger waves are captured, yielding for example steeper crests and shallower troughs.

The electromagnetic calculations are repeated for 3000 176 m-long surface realizations providing robust Monte Carlo sets for statistical analysis of backscatter properties. Both VV and HH-polarized returns are produced by the solution. They are further corrected for the incident field taper (only returns within ± 30 m in ground range from illumination maximum are retained) and other factors to form complex scattering amplitudes S_{VV} and S_{HH} that can be related to the normalized radar cross section [1] as follows (additional factors of 4π or 2π can also be present [5, p. 56]):

$$\langle |S_{\mathrm{pp}}|^2 \rangle = \sigma^0_{\mathrm{pp}} \qquad (1)$$

It should be stressed that these normalizations are performed based on well-known simulation parameters. The whole problem of calibration that is critical for polarimetric radars is therefore a non-issue for the numerical experiment.

3. PROBABILITY DISTRIBUTIONS

Probability density functions (PDF) for sea radar clutter magnitude/power have long been of interest. Notably, deviations of PDFs for either VV or HH magnitude from the Rayleigh curve are observed (meaning that the complex backscattered signal is non-Gaussian), especially at LGA. In particular, PDFs exhibit higher "tails" for large magnitude values, more so for the HH case. Previous numerical simulations [1] reproduced this behavior even when the surfaces did not contain any breaking waves. Another way to get an insight into the sea backscatter properties is to consider a joint PDF for normalized signal magnitudes (or intensities) in VV and HH channels. This is done in Fig. 1 for four incidence angles. It is observed that near nadir (20°) the PDF is quite narrow, running almost diagonally. This means that an occurrence of a particular relative signal level in the VV channel will be accompanied by similar relative level in the HH channel. As the incidence angle increases, the PDFs become more spread-out. At low grazing (85° incidence) the PDF seems to regain a banded shape, indicating that stronger VV echoes will be generally accompanied by stronger HH returns and vice versa. However, now for a given signal level in one channel, there is much broader possible variation range in another channel.

Fig. 2 shows PDFs of phase between the complex HH and VV signals for several incidence angles. For reference, a theoretical prediction for the backscatter by a slightly rough surface (which is a delta-function) can be calculated from the 1st-order Small Perturbation Method (SPM-1), e.g. [6]. The location is dependent on the incidence angle and only the 85° case is shown. It is observed that the phase distributions are unimodal (a local maxima in the negative-phase region, for example, could have been interpreted as a manifestation of a double-bounce-type scattering mechanism, [5, p. 204]). Still, the phase PDFs are substantially non-zero for negative phase values. From the standpoint of the two-scale model [6] (that is expected to apply in the in-

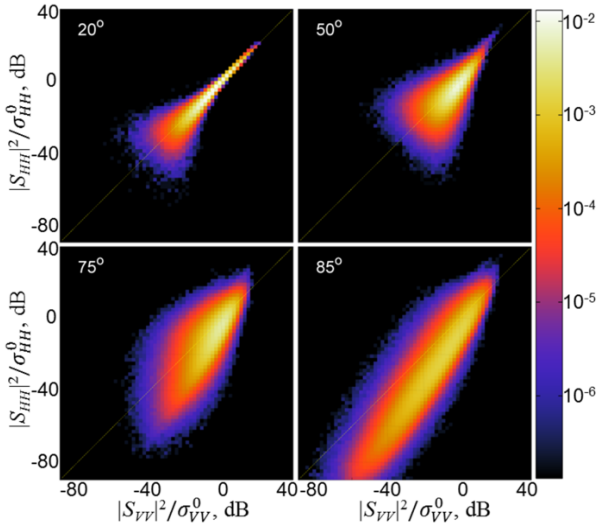

Figure 1. Joint probablility density function of signal intensities in VV and HH channels for 4 different incidence angles. Wind speed is 5 m/s.

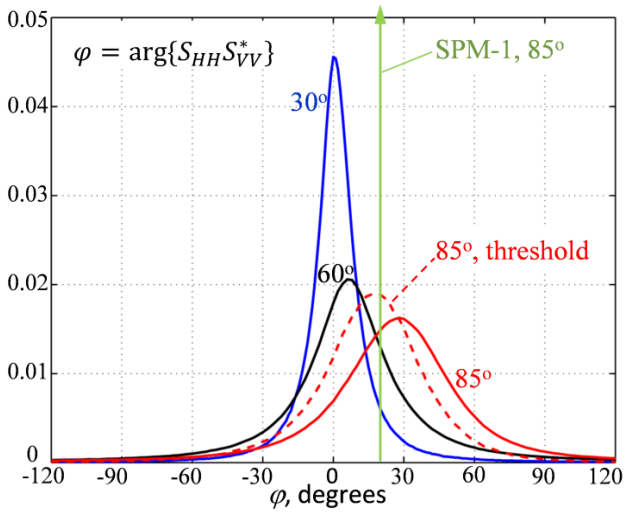

Figure 2. Probablility density function of phase between HH and VV channels for various incidence angles. Wind speed is 5 m/s.

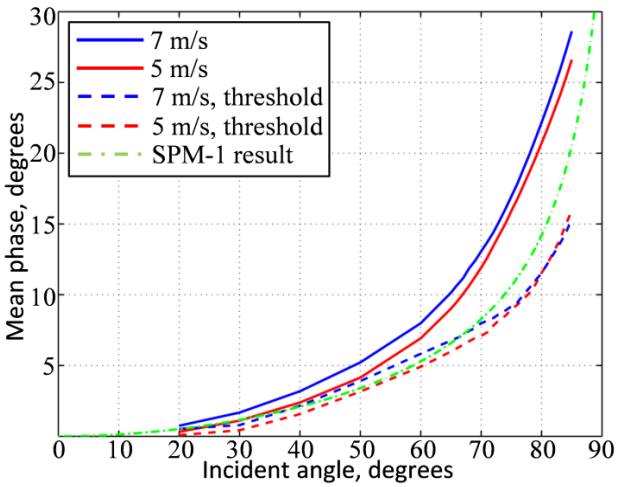

Figure 3. Mean phase vs. incidence angle. 1-st order Small Perturbation method prediction for slightly rough surface is shown for reference.

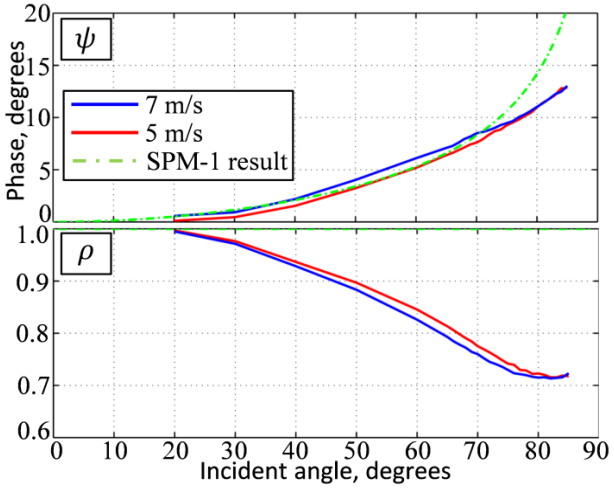

Figure 4. Phase (top) and magnitude (bottom) of complex correlation coefficient in (2) vs. incidence angle.

termediate-incidence backscatter cases), each surface facet scatters as a tilted slightly rough plane. The HH-VV phase differences, as predicted by the SPM-1, will vary depending on the local incidence angle (affected by tilt), but should all be positive. Still, even with the pulse as short as 0.4 m, several facets probably contribute to the signal in a given resolution element, with the contributions summed as complex vectors.

Another issue that affects the phase distributions is noise. At low grazing angles, the backscatter becomes "spiky" (especially at HH), with strong outbursts in some range bins interceded by extensive regions with very low signal levels. In actual radar measurements, such regions will be dominated by thermal noise, affecting phase estimates. This has been verified by artificially adding Gaussian noise to the numerically simulated clutter. Various remedies are possible, such as thresholding or multi-look averaging [7]. Fig. 2 demonstrates the change in the (still noise-free) phase PDF when a 0-dB threshold is applied to HH and VV signals, meaning that only the upper right quadrant with origin at (0 dB, 0 dB) in plots in Fig. 1 contributes

4. AVERAGE QUANTITIES

To further investigate the joint behavior of the VV and HH backscatter vs. incidence angle it is helpful to turn to the distribution moments. Fig. 3 displayed the mean phases for PDFs such as shown in Fig. 2. Two wind speed cases are considered, with the rougher (7 m/s) sea surface showing a consistent if small (1 to 2 degrees) increase in this parameter. A theoretical (SPM-1) prediction for a slightly rough flat surface is again shown for reference. Applying the 0-dB threshold (again, no noise added) results in noticeably lower values, with any distinction between the 5 m/s and 7 m/s curves at LGA being apparently lost. It should be noted that the phase standard deviation is very sensitive to the presence of noise. For example, even with the 0-dB thresholding the estimates for a noise-free backscatter and the 10 dB clutter-to-noise ratio (CNR) case differ by as much as 10°.

Another descriptive quantity to consider is the complex correlation coefficient, cf. (1):

$$\rho_c = \frac{\langle S_{HH} S_{VV}^* \rangle}{(\langle |S_{HH}|^2 \rangle \langle |S_{VV}|^2 \rangle)^{1/2}} \equiv \rho e^{j\psi} \qquad (2)$$

Its phase and absolute value (also called "coherence") are shown in Fig. 4 for the two wind speeds. The behavior of ψ is rather similar to that of the thresholded mean phase in Fig. 3, except that the growth at large incidence angles is slower. The coherence ρ is close to 1 near nadir and then decreases (more so for higher wind speed) as the angle grows. Interestingly, the decline slows around 75° and the curves then level off. The data from simulations at very low grazing angles (below 89°) described in [7] support this observation. Presence of noise (independent in the two channels) does not affect the phase of the correlation coefficient but leads to a drop in the coherence, as can be deduced from (2).

5. POLARIMETRIC $H/\bar{\alpha}$ ANALYSIS

Scene description and classification based on entropy and "alpha-angle" (both arising from eigenvalue decomposition of scattering matrices) has become a popular trend in radar polarimetry [5, p.229]. We examine these quantities for the simulated sea backscatter. The approach starts with determining the eigenvalues λ_1 and λ_2 (2-D case) for the matrix $T = \langle \boldsymbol{k} \cdot \boldsymbol{k}^\dagger \rangle$, with $\boldsymbol{k} = [(S_{HH} + S_{VV}),\ (S_{HH} - S_{VV})]^{\mathrm{T}}/\sqrt{2}$. These are interpreted as contribution levels of different scattering mechanisms. One can define probabilities $P_{1,2} = \lambda_{1,2}/(\lambda_1 + \lambda_2)$ and form the (2-D) polarimetric entropy:

$$H = -[P_1 \log_2(P_1) + P_2 \log_2(P_2)] \qquad (3)$$

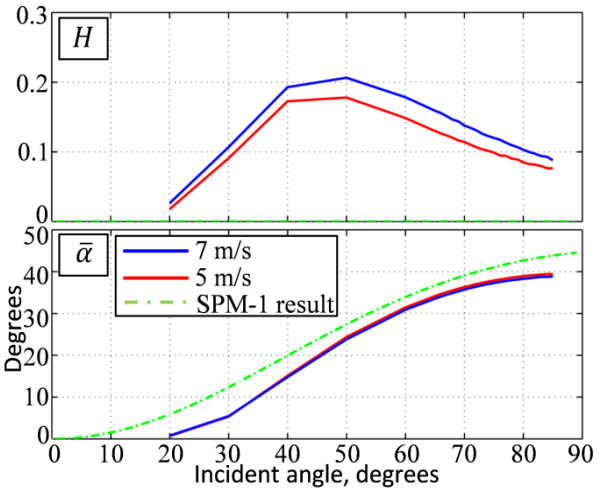

Figure 5. 2-D entropy H (top) and angle $\bar{\alpha}$ (bottom) vs. incidence angle.

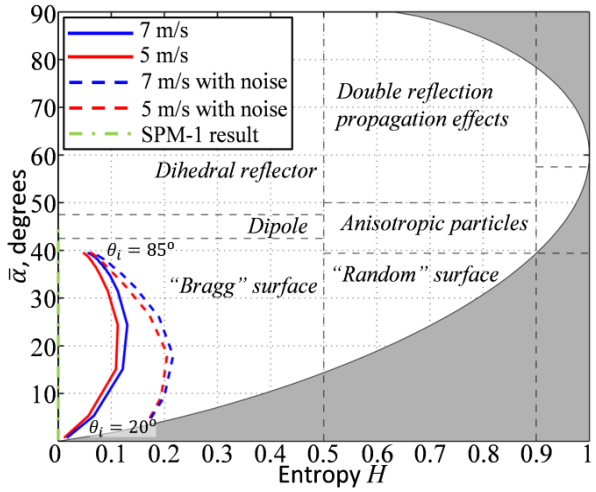

Figure 6. Location of the simulated backscatter parameters in $H/\bar{\alpha}$ classification plane.

Low values are supposed to mean that a single scattering mechanism dominates. The associated unitary eigenvectors are sought in the form $\boldsymbol{u}_{1,2} = [\cos\alpha_{1,2}\ ,\ \sin\alpha_{1,2}\exp(j\delta_{1,2})]^{\mathrm{T}}$ with average angle alpha (deemed to be a signature of the overall scattering mechanism) defined as

$$\bar{\alpha} = P_1\alpha_1 + P_2\alpha_2 \tag{4}$$

We plot both quantities in Fig. 5 for the two wind speeds, again providing the SPM-1 theoretical result for slightly rough surface for reference. Entropy has maximum at an intermediate incidence and is sensitive to the wind speed. The alpha-angle increases monotonically towards grazing and is essentially the same for the two wind speeds. Fig. 6 shows the trajectories of both parameters in $H/\bar{\alpha}$ classification plane as the incidence angle changes (to convert to 3-D space, H in (3) was divided by $\log_2(3)$). The figure also demonstrates significant sensitivity to noise (CNR in the example is 10 dB), mostly through the entropy. While all curves lie in the correct classification section, the $H/\bar{\alpha}$ evolution is, arguably, not particularly informative of the actual scattering processes (e.g. multiple scattering effects are expected to become more prominent towards LGA).

6. CONCLUSION

Direct numerical scattering simulations provide precise tool to study detailed joint properties of polarimetric backscatter. Inherent absence of thermal noise allows establishing the baseline behavior of various parameters; the ability to add noise in a prescribed manner makes the numerical experiment useful for analysis and interpretation of actual field data. Looking at a broad range of incidence angles helps establish some interesting trends, such as flattening of the coherence curve towards grazing. Polarimetric analysis using popular $H/\bar{\alpha}$ decomposition does not seem to provide much insight in the surface scattering processes.

7. ACKNOWLEDGMENT

This work was supported by the US Naval Research Laboratory under the 6.1 Base Research Program (Work Unit 72-4280). It was also supported in part by a grant of computer time from the DoD High Performance Computing Modernization Program at the US Air Force Research Laboratory and the US Army Research Laboratory DoD Supercomputing Resource Centers, and the at the Naval Research Laboratory Distributed Center.

8. REFERENCES

[1] J. V. Toporkov and M. A. Sletten, "Statistical properties of low-grazing range-resolved sea surface backscatter generated through two-dimensional direct numerical simulations," *IEEE Trans. Geosci. Remote Sens.*, vol.45, no. 5, pp. 1181–1197, 2007.

[2] H.-T. Chou and J. T. Johnson, "Formulation of Forward–Backward method using novel spectral acceleration for the modeling of scattering from impedance rough surfaces," *IEEE Trans. Geosci. Remote Sens*., vol. 38, no. 1, pp. 605–607, 2000.

[3] T. Elfouhaily, B. Chapron, K. Katsaros, and D. Vandemark, "A unified directional spectrum for long and short wind-driven waves," *J. Geophys. Res.*, vol. 102, no. C7, pp.15781–15796, 1997.

[4] D. B. Creamer, F. Henyey, R. Schult, and J. Wright, "Improved linear representation of ocean surface waves," *J. Fluid Mech*., vol. 205, pp. 135–161, 1989.

[5] Lee, J.-S. and E. Pottier, *Polarimetric Radar Imaging: from Basics to Applications*, CRC Press, Boca Raton, FL, 2009.

[6] G. R. Valenzuela, "Theories for the interaction of electromagnetic and ocean waves – a review," *Bound.-Lay. Meteorol*., vol. 13, no. 1, pp. 61–85, 1978.

[7] J. V. Toporkov and M. A. Sletten, "Investigation of phase difference statistics of numerically simulated high-resolution HH- and VV-polarized low grazing angle sea backscatter," in *Proc. IEEE International Symposium on Antennas and Propagation*, Spokane, WA, USA, Jul. 2011, pp. 2738–2741.